Supervised Dictionary Learning for Inferring Concurrent Brain Networks

Shijie Zhao, Junwei Han*, *Member, IEEE*,
Jinglei Lv, Xi Jiang, Xintao Hu, Yu Zhao, Bao Ge, Lei Guo, and Tianming Liu*, *Senior Member, IEEE*

***Abstract*—Task-based fMRI (tfMRI) has been widely used to explore functional brain networks via predefined stimulus paradigm in the fMRI scan. Traditionally, the general linear model (GLM) has been a dominant approach to detect task-evoked networks. However, GLM focuses on task-evoked or event-evoked brain responses and possibly ignores the intrinsic brain functions. In comparison, dictionary learning and sparse coding methods have attracted much attention recently, and these methods have shown the promise of automatically and systematically decomposing fMRI signals into meaningful task-evoked and intrinsic concurrent networks. Nevertheless, two notable limitations of current data-driven dictionary learning method are that the prior knowledge of task paradigm is not sufficiently utilized and that the establishment of correspondences among dictionary atoms in different brains have been challenging. In this paper, we propose a novel supervised dictionary learning and sparse coding method for inferring functional networks from tfMRI data, which takes both of the advantages of model-driven method and data-driven method. The basic idea is to fix the task stimulus curves as predefined model-driven dictionary atoms and only optimize the other portion of data-driven dictionary atoms. Application of this novel methodology on the publicly available human connectome project (HCP) tfMRI datasets has achieved promising results.**

***Index Terms*—Task fMRI, group-wise, sparse.**

I. Introduction

TASK-BASED fMRI has been widely used to identify brain regions and brain networks that are functionally involved in a specific task, and has greatly advanced our understanding of functional localizations within the brain [1]–[4]. Traditionally, the general linear model (GLM) [5]–[9] has been the dominant approach to detecting task-evoked networks due to its simplicity, robustness and wide availability. This hypothesis-driven method utilizes the prior knowledge of task or event paradigm together with a canonical hemodynamic response function (HRF) [10] to construct regressors for the general linear model to find activation maps related to a specific task or event-related performance. Although prior work has proven the great advantages of the hypothesis-driven method for task-fMRI data analysis, a possible drawback of GLM is that it focuses on task-evoked or event-evoked brain responses and possibly ignores the intrinsic brain functions [11] involving maintenance of information processing and responding to environmental demands which consumes the largest part of brain energy [12]. On the other hand, a variety of data-driven approaches have been developed, including principal component analysis (PCA) [13], [14] and independent component analysis (ICA) [15]–[19], to explore the intrinsic brain functional networks. Currently, the ICA-based methods have become the dominant approach in data-driven fMRI analysis [20]. The basic assumption of ICA lies in that the fMRI data has been linearly mixed by a set of sources which are spatially (spatial ICA) [15] or temporally (temporal ICA) [17] independent and then the problem becomes one of "unmixing" the spatially or temporally independent fMRI data sources. ICA-based methods have been shown to be useful in resting state fMRI data analysis [21], [22] for which prior paradigm knowledge is not available. However, ICA is not well adapted to the analysis of task and event-related fMRI data [18] for the neglect of task paradigm information. What's more, recent studies [20], [23] proved that the fundamental assumption of independence of the patterns is not guaranteed in practice. Many hemodynamics are correlated with each other due to the interconnections between biological neural networks and the preprocessing steps including smoothing, normalization and realignment [20]. Furthermore, there is not sufficient neural foundation or physical reason for the extracted components corresponding to different brain activity patterns to be statistically independent [24]. Therefore, algorithms which are equipped with other mathematical properties of fMRI data should be explored and developed for data-driven fMRI analysis.

Recently, the dictionary learning and sparse coding methodology developed in the machine learning and pattern recognition fields is purely data-driven and has been shown to be efficient in learning adaptive, over-complete and diverse features for optimal representations [25]–[28]. The aim of sparse representation is to learn a set of basis vectors and represent

Manuscript received February 21, 2015; accepted March 30, 2015. Date of publication April 01, 2015; date of current version September 29, 2015. J. Han was supported by the National Science Foundation of Chinaunder Grant 91120005 and 61473231. X. Hu was supported by the National Science Foundation of Chinaunder grant 61103061 and 61473234, and the Fundamental Research Funds for the Central Universitiesunder grant 3102014JCQ01065. S. Zhao was supported by the Chinese scholarship council. B. Ge was supported by NSFC61403243 & GK201402008. T. Liu was supported by the NIH Career Award (NIH EB006878), NIH R01 DA033393, NSF CAREER Award IIS-1149260, NIH R01 AG-042599, NSF BME-1302089, and NSF BCS-1439051. *Asterisk indicates corresponding author.*

S. Zhao, *J. Han, X. Ji, J. Lv, X. Hu, and L. Guo are with the School of Automation, Northwestern Polytechnical University, Xi'an 710072, China (e-mail: shijiezhao666@gmail.com; junweihan2010@gmail.com; lvjinglei@gmail.com; xintao.hu@gmail.com; lguo@nwpu.edu.cn).

X. Jiang and Y. Zhao are with Department of Computer Science, The University of Georgia, Athens, GA 30602 USA (e-mail: superjx2318@gmail.com; zhaoyu.hust@gmail.com).

B. Ge is with the School of Physics and Information Technology, Shaanxi Normal University, Xi'an 710119, China (e-mail: oct.bob@gmail.com).

*T. Liu is with Department of Computer Science, The University of Georgia, Athens, GA 30602 USA (e-mail: tianming.liu@gmail.com).

Digital Object Identifier 10.1109/TMI.2015.2418734

the original signals as a linear combination of these bases. It should be noticed that only a few bases will be applied when reconstructing a specific signal in these methods which ensured the signals are sparsely represent by the basis vectors. At the same time, a variety of neuroscience studies have reported the sparse response of the neural activity [29]–[31] in brain. Olshaunsen *et al.* [29] observed that sparse linear codes for natural images will develop similar receptive fields to the simple cells in the primary visual cortex. Similarly, Quiroga *et al.* [30] showed that neurons from the medial temporal lobe, amygdala, parahippocampal gyrus, entorhinal cortex, and hippocampus fires selectively and sparsely respond to stimuli. These findings suggest that a sparse set of brain neurons respond to specific stimuli rather than each input. The sparse response principle of brain neural activity coincides with the intrinsic nature of sparse representation methods, which suggests sparse representation may be a possible solution to brain activity detection. Inspired by these exciting results in both fields, several studies applying sparse representation methods [25], [32]–[34] to brain data analysis, including MRI [35], [36], EEG [37]–[40] and fMRI [41]–[48], were proposed. Abolghasemi *et al.* developed a fast incoherent K-SVD method for brain regions activation detection [49] and Eavani *et al.* used sparse representation method to identify functional subnetworks in resting-state fMRI data [50]. Wang *et al.* achieved better detection sensitivity by applying a sparse approximation coefficient prior in ICA decomposition [51]. In addition, Lee *et al.* designed a sparse general linear model framework [20] and Ramezani *et al.* proposed a joint sparse representation analysis (jSRA) to identify common information across multi-task fMRI experiments [52]. These studies demonstrated the advantages of sparse analysis methods. Recently, Lv and Zhang *et al.* [53]–[55] proposed to using dictionary learning method to identify function brain networks based on the assumption that the components of each voxel's fMRI signal are sparse and the neural integration is linear. The basic idea [53]–[55] is to aggregate all of dozens (or hundreds) of thousands of fMRI signals within the whole brain of one subject into a big data matrix, which is subsequently factorized into an over-complete basis signal dictionary and a reference coefficient matrix via dictionary learning and sparse coding algorithms [25]. Particularly, each dictionary column (dictionary atom) represents the BOLD signal pattern of the functional brain activities of a specific brain network and its corresponding reference coefficient vector (a row vector in coefficient matrix) stands for the spatial distribution of this brain network [54], [55]. An important characteristic of this framework is that the decomposed reference coefficient matrix naturally reveals the spatial interaction patterns among inferred brain networks [54], [55]. This novel data-driven strategy naturally accounts for that brain regions might be involved in multiple concurrent functional processes [56]–[58] and thus their fMRI signals are composed of various intrinsic components [55], [59].

Although previous sparse representation based methods have demonstrated great advantages, there are two notable remaining limitations in current data-driven dictionary learning methods: 1) the prior knowledge of task paradigm is not sufficiently utilized yet. Task paradigm information is typically applied after the dictionary learning procedure in selecting the components network of interest through sorting the component time courses based on some similarity criteria [54], [55]. Such method, though useful, does not utilize the task paradigm information directly in the dictionary learning algorithm; 2) the establishment of correspondences among learned task-evoked dictionary atoms or network components in different brains have been challenging. Since these network components are learned in an unsupervised way individually, it is hard to directly compare brain activities in the analysis of multiple subjects. Currently, such comparisons are achieved by combining sorting method and visual check [54], [55], which is quite time consuming and difficult. To address these two limitations, in this paper, we propose a novel supervised dictionary learning and sparse coding method for inferring concurrent functional networks from tfMRI data. The underlying basic idea is to fix the task stimulus curves as predefined model-driven dictionary atoms and only optimize other portion of data-driven dictionary atoms in the dictionary learning procedure. Intuitively, this novel strategy utilizes both of the advantages of model-driven method and data-driven method. The strategy of utilizing task paradigm information directly in the dictionary learning procedure has several major advantages. First, by incorporating paradigm information into the algorithm could avoid the model-driven components converge to local minimum thus it may improve the performance of model-driven networks. Second, it is straightforward to establish the correspondences of the inferred task-related networks across individuals in that the predefined dictionary atoms based on stimulus curves intrinsically offer the match. This novel framework has been applied on the publicly available human connectome project (HCP) tfMRI datasets [60], and meaningful functional networks including both model-driven brain networks and intrinsic brain networks (resting state brain networks) have been identified.

The remaining parts of the paper are organized as follows. The materials and methods are presented in Section II, including data acquisition and preprocessing, theory and algorithm of supervised dictionary learning. Section III provides experimental results and Section IV provides a discussion and conclusion.

II. Materials and Methods

A. Overview

Fig. 1 summarizes the computational pipeline of exploring concurrent functional networks via supervised dictionary learning and sparse coding method. First, for each subject, the whole-brain fMRI signals are extracted and normalized (zero mean and standard deviation of 1), and then aggregated into a signal matrix S (n signals with t time points) (Fig. 1(a)). After that, the signal data matrix is sparsely represented with a signal dictionary D and the corresponding coefficient matrix A by using the novel supervised online dictionary learning and sparse coding methods (Fig. 1(b)). Specifically, we define the constant part of the dictionary D_c (the red part in Fig. 1(b)) as the predefined model-driven task stimulus curves, and only optimize the other part of the data-driven learned dictionary D_l (the green part in Fig. 1(b)) by learning from the fMRI signals. The signal shape of each dictionary column in D

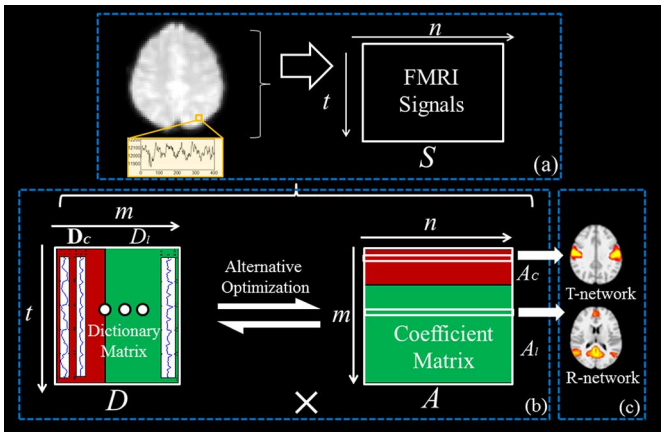

Fig. 1. The computational framework of supervised dictionary learning and sparse coding of whole-brain tfMRI signals for inferring concurrent functional networks. Here T-network and R-network stand for task-evoked network from model-driven networks and resting-state network from data-driven networks, respectively.

represents the BOLD signal pattern of the functional activities of a specific brain network and its corresponding reference coefficient vector in A stands for the spatial distribution of this brain network. Since each row in the coefficient matrix A represents a network distribution in the brain volume, the coefficient matrix A will also be reconstructed into two parts, one representing model-driven task-evoked networks in A_c (red part in Fig. 1(b)), and the other representing data-driven concurrent networks in A_l (green part in Fig. 1(b)).

B. Data Acquisition and Pre-Processing

The data source is the HCP Q1 release [60] and the primary goals of tfMRI datasets in HCP were to identify as many "nodes" as possible in the healthy adult brain that can guide, validate and compare the network connectivity. To achieve these goals, a broad battery of tasks were developed to identify node locations in as a wide range of neural systems as is feasible within realistic time constraints. Therefore, the HCP tfMRI datasets provide one of the most systematic and comprehensive mapping between connectome-scale functional networks and tasks over a large population of subjects in the literature so far. In the HCP Q1 release data set, the tfMRI data were provided for 68 participants with 7 task designs and A brief description of each task could be found in supplemental materials.

The detailed acquisition parameters of HCP tfMRI data are as follows: 90×104 matrix, 220 mm FOV, 72 slices, TR $= 0.72$ s, TE $= 33.1$ ms, flip angle $= 52°$, BW $= 2290$ Hz/Px, in-plane FOV $= 208 \times 180$ mm, 2.0 mm isotropic voxels. For tfMRI images, the preprocessing pipelines included motion correction, spatial smoothing, temporal pre-whitening, slice time correction, global drift removal. More detailed task description and task paradigm could be found in literature [60].

C. Supervised Dictionary Learning and Sparse Representation

Dictionary learning and sparse representation is an unsupervised learning algorithm which aims to find a basis set in the data and learn sparse coefficients to sparsely represent the data. Although these methods [20], [55], [52], [53] have shown promising results, many studies which combined sparse coding with some constraints [28], [70], [71] have achieved inspiring results in some cases. Wright and his colleagues [26] constrained different classes of test samples as dictionary for face recognition to improve the classification result and Zheng and his colleagues utilized graph information in sparse coding to enhance image representation. Recent study has suggested that the real potential of sparse coding methods for fMRI analysis will increase when the prior information is incorporated into the estimation scheme [72], if possible. In this paper, we propose a novel supervised dictionary learning and sparse coding method to incorporate task paradigms for inferring concurrent functional networks from tfMRI data. The underlying basic idea is to fix the task stimulus curves as predefined model-driven dictionary atoms and only optimize other portion of data-driven dictionary atoms in the dictionary learning procedure. Specifically the predefined model-driven dictionary atoms (the constant part $\mathbf{D}_c$ in supervised dictionary learning procedure) are constructed by the convolution of task paradigms and the haemodynamic response function (HRF) using the FSL toolbox [6]. The number of the fixed atoms is based on the number of stimuli applied in the task. In our experiments, there are two constrained dictionary atoms in emotion, gambling, language, relational and social task datasets, there are six fixed atoms in motor task dataset and four constrained dictionary atoms in working memory task dataset, and the dictionary size is 400 at the same time. The fixed dictionary atom number is consistent with the number of stimuli and usually occupies less than 1% portion in the total dictionary atoms. Our rationale to fix these numbers of dictionary atoms is similar with GLM in that part of the activated brain voxel activities should follow the stimuli paradigm. Given the tfMRI signal matrix $S \epsilon \mathbb{R}^{t \times n}$ (Fig. 1(a)), where n is the number of voxels in a subject's brain and t is the number of fMRI time series points, each tfMRI signal in S is modeled as a sparse linear combination of atoms of a learned basis dictionary D (Figs. 1(b)), i.e., $s_i = D \times A_i$ and $S = D \times A$, where A is the coefficient matrix for sparse representation. Particularly, the signal shape of each dictionary atom in D represents the functional activities of a specific brain network and its corresponding reference coefficient vector in A stands for the spatial distribution of this brain network [55]. In this work, we aim to learn a meaningful and over-complete dictionary $D \epsilon \mathbb{R}^{t \times m} (m > t, m << n)$, for the sparse representation of S. Specifically,

$$D = [\mathbf{D}_c, D_l] \epsilon \mathbb{R}^{t \times m}, \mathbf{D}_c \epsilon \mathbb{R}^{t \times m_c}, D_l \epsilon \mathbb{R}^{t \times m_l} \quad (1)$$

where $\mathbf{D}_c$ is the predefined model-driven constant dictionary atoms and D_l is the data-driven dictionary atoms from the tfMRI signals and m_c and m_l are atom numbers of constant dictionary and learned dictionary, respectively. For the signal set $S = [s_1, s_2, \ldots s_n] \epsilon \mathbb{R}^{t \times n}$, the empirical cost function is defined in (2) by averaging the loss of regression of n signals.

$$f_n(D) \triangleq \frac{1}{n} \sum_{i=1}^{n} \ell(s_i, [\mathbf{D}_c, D_l]) \quad (2)$$

The loss function is defined in (3) with a ℓ_1 regularization that yields to a sparse resolution of A_i and here λ is a regularization parameter to trade-off the regression residual and sparsity level.

$$\ell(s_i, D) \triangleq \min_{A_i \epsilon \mathbb{R}^m} \frac{1}{2}||s_i - [\mathbf{D}_c, D_l]A_i||_2^2 + \lambda||A_i||_1 \quad (3)$$

As we focus on the fluctuation shapes of basis fMRI activities and aim to prevent D from arbitrarily large values, the columns $d_1, d_2, \ldots\ldots d_m$ are constrained by (4).

$$C \triangleq \left\{ D \epsilon \mathbb{R}^{t \times m} \; s.t. \; \forall j = 1, \ldots m, d_j^T d_j \leq 1 \right\} \quad (4)$$

$$\min_{D \in C, \alpha \epsilon \mathbb{R}^{m \times m}} \frac{1}{2}||S - [\mathbf{D}_{\mathrm{c}}, D_l]A||_F^2 + \lambda||A||_{1,1} \quad (5)$$

In brief, the problem of supervised dictionary learning can be rewritten as a matrix factorization problem in (5) [25]. In order to solve this problem, we adopted the modified online dictionary learning and sparse coding method (SPAMS package in [25]), that is, the newly developed/rewrote codes of supervised dictionary learning for this work. The whole supervised dictionary learning and sparse coding algorithm pipeline is summarized in Algorithm 1 below.

Algorithm 1. The supervised online dictionary learning and sparse coding.

Input: $S = [s_1, s_2, \ldots s_n] \epsilon \mathbb{R}^{t \times n}$, $\lambda \epsilon \mathbb{R}$, $D_0 = [\mathbf{D}_c, D_{l0}] \epsilon \mathbb{R}^{t \times m}$ (initial dictionary, $\boldsymbol{D}_c$ is predefined, D_{l0} is randomly generated, T (number of iteration).

1: for iter $= 1$ to T
2: $\quad i = \text{iter}\%n \; (T > n)$
3: $\quad$ Draw s_i from S
4: $\quad$ Sparse coding using Least-angle Regression:

$$A_i \triangleq \underset{\mathrm{A_i} \epsilon \mathbb{R}^{\mathrm{m}}}{\operatorname{argmin}} \frac{1}{2} \left|\left|s_i - \mathbf{D}_{(\mathbf{t}-\mathbf{1})} A_i\right|\right|_2^2 + \lambda||A_i||_1$$

5: $\quad$ Update $D_{l(t)}$ but keep $\mathbf{D}_{\mathrm{c}}$ constant:

$$D_{(t)} \triangleq \underset{D_l \epsilon \mathrm{C}}{\operatorname{argmin}} \frac{1}{2} \left|\left|s_i - D_{(t-1)} \mathbf{A_i}\right|\right|_2^2 + \lambda||\mathbf{A_i}||_1 \quad \left(D_{(t-1)} = \left[\mathbf{D}_{\mathrm{c}}, D_{l(t-1)}\right]\right)$$

6: end for
7: Return D and A;

D. Identification of Functional Networks

With our method, each tfMRI signal matrix $S \epsilon \mathbb{R}^{t \times n}$ (Fig. 1(a)) is modeled as a sparse linear combination of atoms of a learned basis dictionary D(Figs. 1(b)), i.e., $s_i = D \times A_i$ and $S = D \times A$, where A is the coefficient matrix for sparse representation. Each atom in the dictionary represents the functional activities of a specific brain network and each dimension of its corresponding reference coefficient vector associated with a specific atom (the corresponding row in A) stands for the spatial distribution of this brain network [55]. With the assistance of the preserved voxel index, each row in A can be mapped back to the brain volume space, which represents the spatial distribution of each dictionary atom of D, as shown in Fig. 1(c).

Based on the predefined constant task stimulus curves in the dictionary, it is quite straightforward to map out all the stimulus-specific task-evoked brain networks from A_c. At the same time, other concurrent networks, such as resting state networks, can be adaptively learned and mapped from A_l. Since these data-driven networks are learned in an unsupervised way individually, it is hard to group-wisely interpret brain activities from D_l. Therefore, a spatial matching method is employed to compare those data-driven networks in A_l with the well-established resting state network (RSN) templates in the literature [74]. The spatial matching rate is defined as:

$$R(X, T) = \frac{|X \cap T|}{|T|} \quad (6)$$

where X is the A_l component network's spatial map and T is the RSN template.

III. Experimental Results

The proposed framework has been applied on the seven concurrent HCP tfMRI datasets respectively, that is, emotion/gambling/language/motor/relational/social and working memory tasks. The uncovered model-driven networks learned using our methods are examined in Section A, and other networks which are corresponding with D_l are related to data-driven networks, as shown in Section B.

A. Learned Group-Wise Consistent Model-Driven Functional Networks

With our method, we can reconstruct the signal shapes of these fixed model-driven dictionary atoms which can be regarded as model-driven networks. For instance, in the HCP motor task dataset, the fixed stimulus patterns and their time series curves are shown in Fig. 2(a) (I). With our methods, we can reconstruct the distributions of $\mathbf{D}_{\mathrm{c1}} - \mathbf{D}_{\mathrm{c6}}$, which can be regarded as task-related networks (represented by M1-M6). Their spatial distributions are shown in the red panels of Figs. 2(a) (II-IV). Specifically, Figs. 2(a) (II-III) show individual spatial maps of two randomly selected subjects, and Fig. 2(a) (IV) show the group-wise averaged one across the whole population. For comparison, the GLM-based activation detection results are also shown in the blue panes of Figs. 2(a) (II- IV) respectively. It is interesting that our detected networks are quite similar with the GLM-based activation patterns and also are quite group-wise consistent. In total, we identified 2, 2, 2, 2, 2, 5, and 4 model-driven networks for emotion (E1-E2 in Fig. 2(b)), gambling (G1-G2 in Fig. 2(b)), language (L1-L2 in Fig. 2(b)), motor (M1-M6 in Fig. 2(b)), social (S1-S2 in Fig. 2(b)) and working memory (W1-W4 in Fig. 2(b)) tasks, respectively. Interestingly, similar with the GLM-based activation patterns, these model-driven networks across all of the HCP Q1 release subjects are quite consistent and stable as shown in Fig. 2(b).

We further compared the averaged model-driven networks across all subjects with the corresponding group-wise GLM activation maps in Fig. 3(a) and Fig. 3(b). Fig. 3 clearly shows that the averaged model-driven networks are quite similar to the corresponding group-wise GLM activation maps. Through

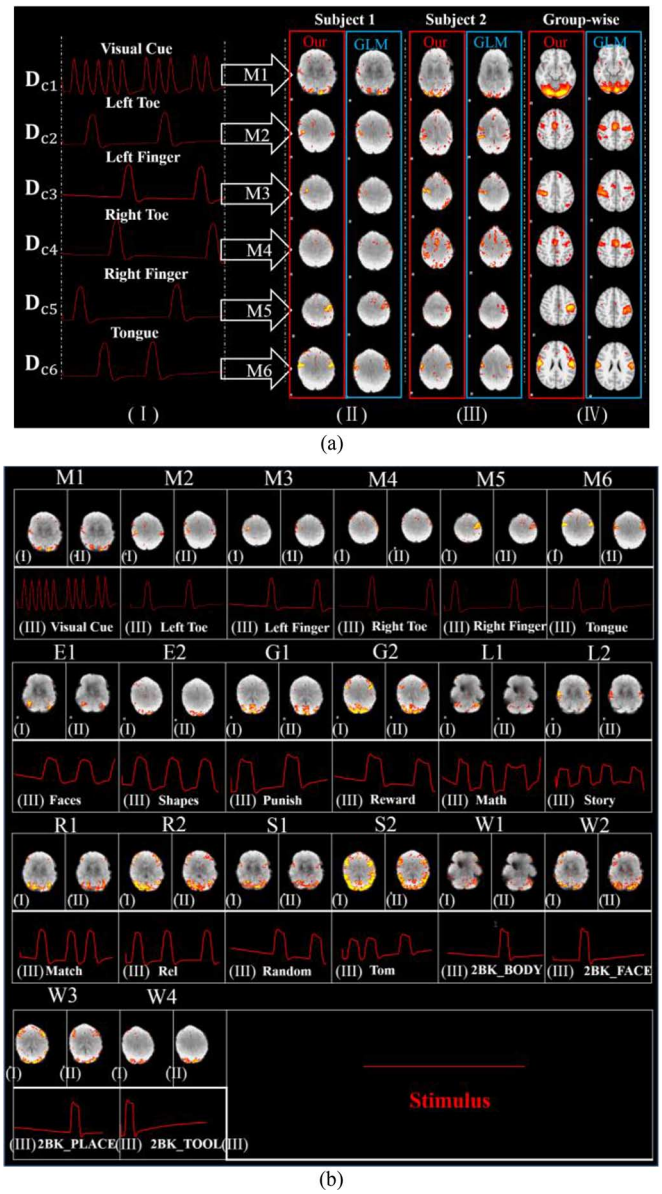

Fig. 2. (a) The model-driven networks in HCP motor dataset. (I) The six fixed stimulus curve in $\mathbf{D}_c$. (I-IV) Red panels are the corresponding motor task evoked networks (M1-M6) reconstructed with our method. Blue panels are the activation detected by GLM method. (II) and (III) are two randomly selected subjects. (IV) is the group-wise results. (b) The model-driven networks in all HCP task datasets and the corresponding GLM-derived activation maps in one randomly selected subject. (I) is the model-driven network reconstructed with our method, (II) is the activation map detected by GLM method and (III) is the fixed stimulus curve in $\mathbf{D}_c$. E1-E2, G1-G2, L1-L2, M1-M6, R1-R2, S1-S2 and W1-W4 correspond to the fixed stimulus paradigm in emotion, gambling, language, motor, relational, social and working memory task.

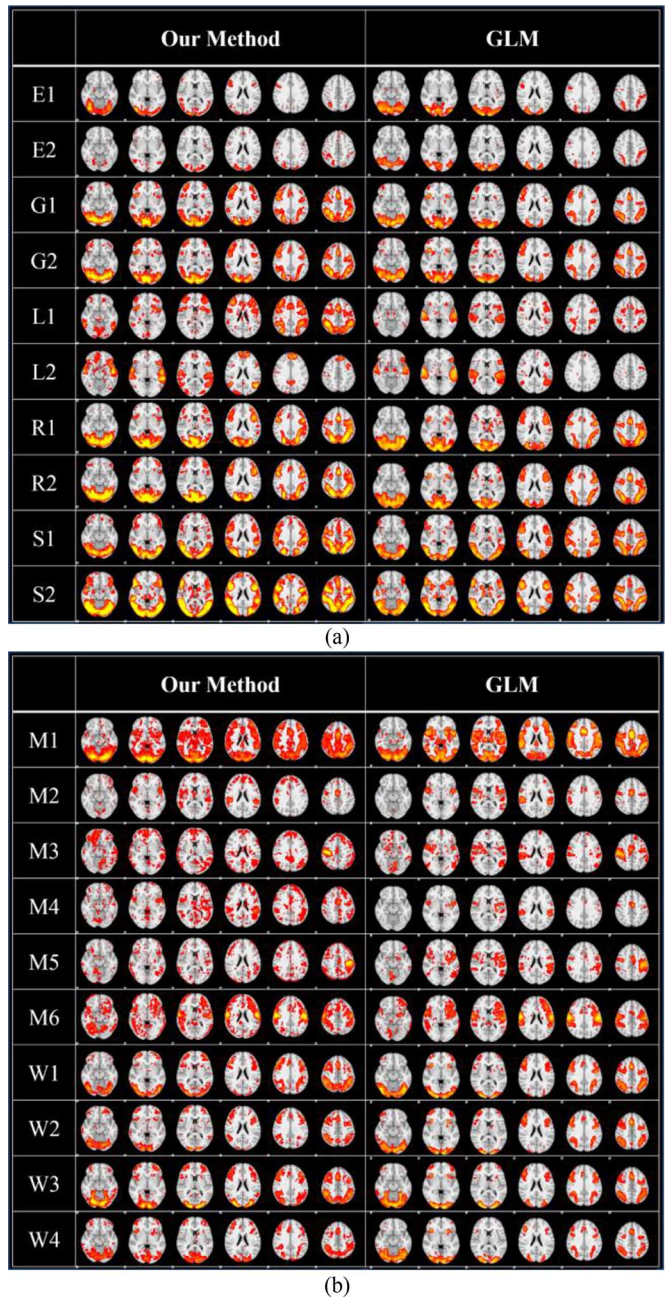

Fig. 3. Group-wise average model-driven networks by our method and the group-wise GLM-derived activation maps in seven tfMRI datasets. (a) Group-wise average result of model-driven networks by our method and the group-wise GLM-derived activation maps in emotion, gambling, language, relational, social task. (b) Group-wise average result of model-driven networks by our method and the group-wise GLM-derived activation maps in motor and working memory task.

the comparison, the high spatial overlap and group-wise consistence suggest that our method can detect quite meaningful and reliable model-driven networks. Quantitatively, the mean spatial overlap rate of group-wise averaged model-driven networks with group-wise GLM activation map is detailed in Supplemental Table I and Supplemental Table II. Supplemental Table III and Supplemental Table IV show the spatial overlap rates of model-driven networks with GLM activation maps across all HCP Q1 release subjects, represented as mean $\pm$ std. These high overlap rate results demonstrated that the supervised dictionary learning method can effectively recover model-driven/task-evoked networks.

B. Learned Group-Wise Consistent Data-Driven Functional Networks

With our method, we could simultaneously discover intrinsic brain networks in D_l. Limited by current knowledge, we only take well-established RSN templates [74] as examples. Since these networks are learned in an unsupervised way individually, it is hard to group-wisely interpret brain activities from D_l.

Therefore, we examined the similarity between the dictionary atom's spatial patterns and the well-established RSN templates in the literature [74]. Specifically, we defined the similarity as the spatial overlap rate which is characterized in (6). To discover the well-established RSN networks in [74], we went through all of the decomposed dictionary atoms in D_l across all of the HCP Q1 tfMRI datasets and quantitatively and visually compared the dictionary atom's spatial patterns with the well-established RSN templates and identified nine consistent RSNs in all of the HCP Q1 tfMRI datasets. Figs. 4(a) shows the reconstructed default mode network (DMN) of ten randomly selected subjects across seven tfMRI datasets and Figs. 4(b) shows the reconstructed frontal network of ten randomly selected subjects across seven tfMRI datasets. It is evident that these RSNs are quite consistent and similar to the templates across all subjects and tfMRI datasets. In addition, we evaluated the group-wise average of all detected RSNs across all of the HCP Q1 subjects, as shown in Fig. 4(c). The quantitative measurement of mean spatial overlap rate of nine group-wise averaged RSNs detected via our method with RSN templates is as high as 0.84 as detailed in Supplemental Table V. Supplemental Table VI shows the spatial overlap rates of nine RSNs detected via our method across all HCP Q1 release subjects. From these results, we can see that the group-wise average of these RSNs are quite similar with the well-established RSN templates [74] across all the HCP Q1 tfMRI datasets. This result further demonstrated that our method is capable of simultaneously inferring other concurrent meaningful networks like RSNs that might interact with the model-driven networks, which is a major advantage of this framework.

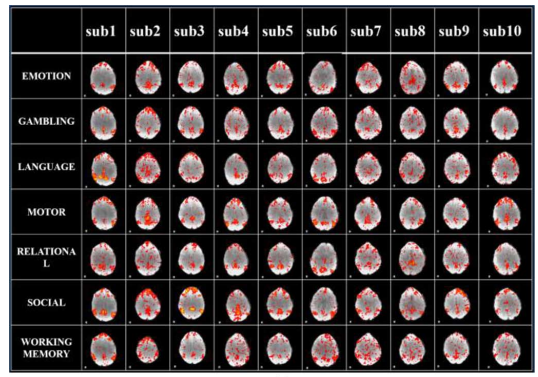

(a)

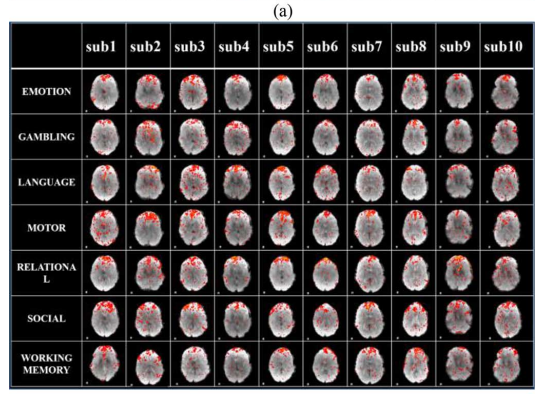

(b)

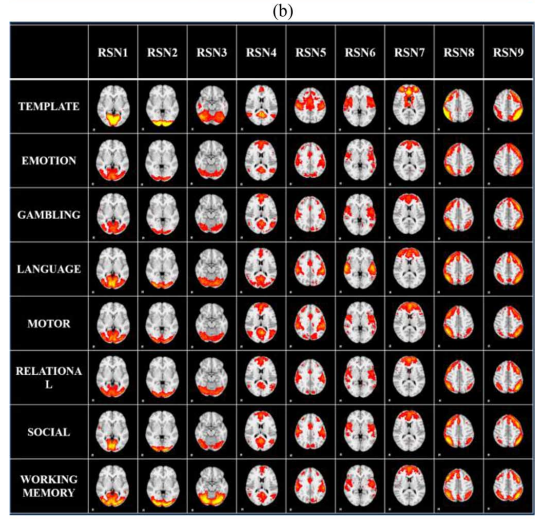

(c)

Fig. 4. The detected nine resting state networks in seven HCP Q1 tfMRI datasets. (a) The reconstructed DMN network from 10 randomly selected subjects in seven HCP Q1 tfMRI datasets. Limited by the space, only the most informative slice overlaid on the mean fMRI image of each subject is shown. The color scale of spatial maps detected by our method range from 0.1 to 10. (b) The reconstructed frontal network from 10 randomly selected subjects in seven HCP Q1 tfMRI datasets. (c) The group-wise averages of the results by our method and the templates for the nine RSN networks in all HCP Q1 tfMRI datasets. For the group-wise average results and templates, only the most informative slice, which is overlaid on the MNI152 template image, is shown as the spatial map of the specific RSN.

C. *Parameters in Supervised Dictionary Learning*

Two crucial parameters in our proposed method as well as in the standard dictionary learning procedure are the dictionary size k and the sparsity level constraint λ. In the dictionary learning field, it is still an open question to optimize these two parameters. Therefore, in this work, these parameters are set experientially. In order to evaluate the effects of different parameter settings on our final results, different combinations of parameters were explored to examine the reproducibility and stability of our method. Specifically, we applied the same supervised dictionary learning pipeline on multiple randomly selected subjects (one used here as an example) with combinations of different parameters in motor tfMRI dataset. In order to separately determine the influence of the parameter size k and the sparsity level constraint λ, we first fixed the dictionary size as 400 and we alternate the regularization parameter λ from 0.05 to 2.05. The derived model-driven networks are shown in Supplemental Fig. 1(a) and the derived resting state networks from the data-driven part (DMN and FRONTAL networks used here as examples) are shown in Supplemental Fig. 1(c). It is evident that both the model-driven networks and data-driven networks are not sensitive to the parameter of regularization parameter λ in a range of parameters and the detected brain networks are stable and robust. Meanwhile, in another experiment, the regularization parameter λ is fixed and size k alternates from 300 to 1000. The derived model-driven networks are also shown in Supplemental Fig. 1(b) and the derived DMN and frontal networks are shown in Supplemental Fig. 1(d). From Supplemental Fig. 1, we can clearly see that although the parameter alternation will cause slight spatial variation for the derived model-driven and data-driven networks, the overall patterns are consistent and stable in a large range of parameter settings. Thus, these results

indicate that our method is stable and reproducible in simultaneously reconstructing meaningful model-driven and data-driven networks.

In the current stage, there is no golden criterion for parameter selection and we have to set these parameters experimentally. Note that, learning a meaningful and over-complete dictionary $D \epsilon \mathbb{R}^{t \times m}$ should satisfy $m > t, m << n$ [25], which means the lower boundary of the dictionary size should be t (the number of fMRI time series points). However, the dictionary size should not be too big in order to avoid redundant information and the spatial pattern to be too sparse. Based on our observation, the dictionary size satisfying $t < k$ (dictionary size) $< 2t$ usually gives good result [55]. For instance, in our experiments, there are 284 fMRI time series points in motor task and the dictionary size $k < 600$ gives good result as shown in Supplemental Fig. 1(b) and Supplemental Fig. 1(d). The parameter λ will also influence the sparsity and scale of components regions. We usually set it no higher than 1 to achieve good reconstruction networks which exhibit meaningful spatial distributions.

D. Comparison With Conventional Dictionary Learning Method

We also conducted conventional dictionary learning methods [55] on these datasets as control experiments. In order to eliminate the influence of parameter settings, we adopted the same parameters as supervised dictionary learning. Since conventional dictionary learning is a purely data-driven method and the network components are learned individually, there is no correspondence between multiple subjects. Therefore, we adopted the sorting and matching method in [55] to characterize the task-related and intrinsic (take resting state networks as examples) brain networks. Specifically, we examined the similarity between the dictionary atom's spatial distributions and the network templates (including the corresponding GLM network templates and the well-established RSN templates [74]) and identified the atom with the largest similarity as the corresponding network component. Similarly, we defined the similarity as the spatial overlap rate which is characterized in (6). With conventional dictionary learning method, we also identified the same number of task-related brain networks and resting state brain networks. Supplemental Fig. 2 (2) shows the reconstructed task-related networks in motor task via our method and conventional dictionary learning method in one randomly selected subject in motor task dataset. From this figure, we can see that the brain networks detected via our supervised dictionary learning method show slightly more overlap with GLM activation map than control experiments. The detailed quantitative measurement of spatial overlap rate between the dictionary atoms and templates are shown in Supplemental Tables VII–X. Supplemental Table VII shows the spatial overlap rates between group-wise averaged task-related dictionary atoms and the group-wise GLM activation maps and Supplemental Table VIII shows the spatial overlap rates of task-related dictionary components and GLM activation maps in individual data sets, represented as mean $\pm$ std. Similarly, Supplemental Table IX shows the spatial overlap rates between the group-average dictionary components and the RSN templates and Supplemental Table X shows the spatial overlap results in individual datasets. Supplemental Fig. 3 shows the group-wise averaged task-related and resting state brain networks reconstructed in control experiments.

From both spatial and quantitative results, we can see that task-related components reconstructed by our method have shown higher spatial overlap rates with GLM activation maps in both group-averaged results and individual results than control experiments. Results also show that the RSN networks detected by our method illustrate slightly higher spatial overlap rates than control experiments. The reason may lies in that with fixed dictionary atoms in the dictionary learning procedure, the algorithm could avoid the components converging to local minimum thus it may improve the reconstruction performance of both model-driven networks and intrinsic networks.

E. Comparison With ICA Method

We further compared our results with well-established independent component analysis (ICA) method [75] of whole-brain fMRI signals. Since ICA is also a purely data-driven method and there is no correspondence among multiple subjects, we adopted the similar strategy in Section III.D to characterize the task-related and RSN brain networks. We went through all of the independent components and labeled the component which shows the largest spatial overlap rates with templates as the corresponding network component. For comparison purpose, Supplemental Fig. 2(4) shows the identified task-related components via ICA method in motor task dataset of the same subject. It is clear to see that the task-related network components detected via ICA method are quite different with GLM activation maps and other methods, and it seems ICA method failed to characterize different task-related network components in motor task dataset of this subject. We further compared the group-wise averaged task-related networks across all subjects with the group-wise GLM activation maps in Supplemental Fig. 4(a) and Supplemental Fig. 4(b). It seems that ICA method is able to characterize task-related networks in some simple task with fewer stimuli like emotion, gambling, language, relational and social task dataset. However, it poses difficulty in detecting task-related in some complex task data like motor and working memory task datasets which have more stimuli. For comparison purpose, the detailed quantitative measurement of spatial overlap rate between the independent components and templates are shown in Supplemental Table XI–XII. From these results, we can see that our supervised dictionary learning method shows great superiority in detecting task-related brain networks in tfMRI datasets. The reason may lie in that our supervised dictionary method takes the advantage of task paradigm information in the learning procedure and improved the performance of detecting task-related brain networks.

Supplemental Fig. 4(c) shows the characterized group-wise averaged RSN networks via ICA method across all seven HCP task datasets. Similar with our method, ICA method also characterized 9 consistent resting state brain networks across all the HCP task fMRI datasets. Supplemental Table XIII and Supplemental Table XIV illustrate the quantitative overlap results between the ICA components and RSN templates. From both spatial patterns and quantitatively results, we can see that our su-

pervised dictionary learning method showed similar ability in detecting intrinsic brain networks as ICA method.

F. Supervised Dictionary Learning Method With Only Fixed Atoms

We also conducted experiments of supervised dictionary learning method with only fixed atoms (we call them Dctest experiments) on HCP tfMRI datasets to examine the influence of the data-driven part dictionary in our method. Specifically, in each subject's tfMRI dataset, the predefined model-driven dictionary atoms (the constant part $\mathbf{D}_c$ in supervised dictionary learning procedure) are fixed as dictionary and we utilized it to learn the coefficient matrix. Supplemental Fig. 2(3) shows the identified task-related components via Dctest method in motor task dataset of the same subject. We also characterized the group-wise task-related networks in Supplemental Fig. 5. From these figures, we can see that the task-related networks reconstructed by Dctest method are quite similar to GLM activation maps. The quantitative spatial overlap measurements are shown in Supplemental Table XV and Supplemental Table XVI.

After comparing these results with our method, we can see that the augment of data-driven part dictionary in our supervised dictionary learning method only results in little negative influence on the detection of task-related brain networks but it brings in the ability to detect intrinsic brain networks simultaneously.

IV. Discussion and Conclusion

We have proposed a hybrid model-driven and data-driven algorithm to explore the task-related and intrinsic brain networks in HCP Q1 task fMRI datasets. The proposed method has several advantages. First, compared with traditional GLM approaches and Dctest method, our method could simultaneously estimate the model-driven and data-driven components, which demonstrates the existence of intrinsic brain networks in task fMRI datasets as pointed in [12], [55]. Detailed experimental results of reconstructed model-driven networks (Figs. 2 and 3) and intrinsic brain networks (such as resting state networks in Fig. 4) have supported our conclusion. In addition, the sparse representation and dictionary learning based method coincides with the sparsity principle of the neural response thus it is more feasible to perform task fMRI data analysis. Thirdly, compared with conventional dictionary learning methods [54], [55] and ICA methods [75], it is straightforward to establish the correspondences of the inferred task-related networks across individuals for the predefined dictionary atoms based on stimulus curves intrinsically offer the match. What's more, compared with purely data-driven methods like ICA and conventional dictionary learning, with the fixed dictionary atoms in the dictionary learning procedure, the algorithm could avoid the components converge to local minimum thus it may further improve the reconstruction performance, especially the task-related network components as detailed in Section III.

Notably, there are still some questions need to be further explored about our method in the future. For instance, parameters should be carefully selected for our novel approach, including the sparsity level constraint λ and the dictionary size k. Although, experiments results in Section III.C have demonstrated that our method is robust and effective among a range of parameter settings and a small portion of fixed atoms is working well, our ongoing work is trying to optimize these parameters in a theoretic or experimental framework. Limited by current knowledge, in this paper, we have focused on the characterization of well-known categories of dictionary atoms including the GLM-related and resting-state network components, as shown in Sections III.A and III.B. It should be noted that there are many other potentially important and meaningful network components [73] to be examined and characterized in the future. Furthermore, although experiment results on HCP tfMRI datasets which is one of the most systematic and comprehensive mapping between connectome-scale functional networks and tasks over a large population of subjects have demonstrated the robustness of our novel method, we should also adopt simulations as a validation tool in the future. However, the simulation should be carefully designed to mimic the brain activities.

In this paper, we have focused on simultaneously estimating the model-driven networks and intrinsic brain networks using supervised dictionary learning in tfMRI data and the detailed experiments results in Section III have demonstrated the superiority of this newly developed method. However, the methods could be further enhanced and improved if the computation cost could be reduced. In the current stage, we aggregated the whole-brain signals into a big signal matrix from which to learn an over-complete dictionary basis. However, many voxels showed similar activity patterns which suggest that appropriate sampling method may boost our method. Besides, algorithms which effectively solve the ℓ_1 norm regulation problem will further advance our method. For instance, Huang and his colleagues [75], [76] proposed a Composite Splitting Algorithm (CSA) to tackle composite regularization problems and achieved promising results. The combination with these advanced algorithms might deserve a try in the future. What's more, in our current experiments, we only put ℓ_1 regularization to the coefficient matrix which may neglect the temporal property and thus limit the method's ability. Caballero and his colleagues [78] introduced temporal gradient sparsity into sparse representation model and greatly improved reconstruction performance. This suggests that combing temporal sparsity into our method may be another future direction to explore.

In summary, we have presented a novel supervised dictionary learning method for brain activity detection. By predefining task stimulus curves as the constant part of the learned over-complete dictionary, our method is capable of accurately detecting task-related functional networks. Meanwhile, the data-driven learning part of the dictionary atoms can sufficiently account for those intrinsic brain networks that do not necessarily follow the task stimulus curves like the resting state networks. In summary, our proposed approach takes both of the advantages of model-driven methods and data-driven methods, and can effectively infer concurrent and heterogeneous functional networks for systematic assessments of functional activities in tfMRI data. Motivated by our exiting results, we believe it will be invaluable to apply hybrid data-driven fMRI analysis method in other future HCP release datasets, as well as from other task fMRI datasets,

and further assess possible alterations of intrinsic brain components and interactions in brain disorders such as Alzheimier's disease and Schizophrenia.

REFERENCES

[1] N. K. Logothetis, "What we can do and what we cannot do with fMRI," *Nature*, vol. 453, pp. 869–878, Jun. 2008.

[2] K. J. Friston, "Modalities, modes, and models in functional neuroimaging," *Science*, vol. 326, pp. 399–403, Oct. 2009.

[3] M. A. Just *et al.*, "Functional and anatomical cortical underconnectivity in autism: Evidence from an FMRI study of an executive function task and corpus callosum morphometry," *Cerebral Cortex*, vol. 17, no. 4, pp. 951–961, Jun. 2007.

[4] W. Du *et al.*, "High classification accuracy for schizophrenia with rest and task FMRI data," *Front. Human Neurosci.*, vol. 6, p. 145, Jun. 2012.

[5] P. A. Bandettini *et al.*, "Processing strategies for time-course data sets in functional MRI of the human brain," *Magn. Reson. Med*, vol. 30, no. 2, pp. 161–173, 1993.

[6] K. J. Friston *et al.*, "Statistical parametric maps in functional imaging: A general linear approach," *Human Brain Mapp.*, vol. 2, no. 4, pp. 189–210, 1994.

[7] K. J. Friston *et al.*, "Event-related FMRI: Characterizing differential responses," *Neuroimage*, vol. 7, no. 1, pp. 30–40, Jan. 1998.

[8] C. F. Beckmann, M. Jenkinson, and S. Smith, "General multilevel linear modeling for group analysis in FMRI," *Neuroimage*, vol. 20, no. 2, pp. 1052–1063, Oct. 2003.

[9] K. J. Worsley, "An overview and some new developments in the statistical analysis of PET and fMRI data," *Human Brain Map.*, vol. 5, no. 4, pp. 254–258, 1997.

[10] W. D. Penny, K. J. Friston, J. T. Ashburner, S. J. Kiebel, and T. E. Nichols, "Statistical parametric mapping: The analysis of functional brain images," in *The Analysis of Functional Brain Images*. New York: Academic, 2011.

[11] M. E. Raichle, "Two views of brain function," *Trends Cognitive Sci.*, vol. 14, no. 4, pp. 180–190, Apr. 2010.

[12] L. Sokoloff *et al.*, "The effect of mental arithmetic on cerebral circulation and metabolism," *J. Clin. Invest.*, vol. 34, pp. 1101–1108, Jul. 1955.

[13] A. H. Andersen, D. M. Gash, and M. J. Avison, "Principal component analysis of the dynamic response measured by fMRI: A generalized linear systems framework," *Magn. Reson. Imag.*, vol. 17, no. 6, pp. 795–815, Jul. 1999.

[14] R. Viviani *et al.*, "Functional principal component analysis of fMRI data," *Human Brain Map.*, vol. 24, no. 2, pp. 109–129, Oct. 2004.

[15] M. J. McKeown *et al.*, "Spatially independent activity patterns in functional MRI data during the stroop colornaming task," *PNAS*, vol. 95, no. 3, pp. 803–810, 1998.

[16] J. V. Stone, J. Porrill, N. R. Porter, and I. D. Wilkinson, "Spatiotemporal independent component analysis of event-related fMRI data using skewed probability density functions," *Neuroimage*, vol. 15, no. 2, pp. 407–421, Feb. 2002.

[17] B. B. Biswal and J. L. Ulmer, "Blind source separation of multiple signal sources of fMRI data sets using independent component analysis," *J. Comput. Assist. Tomogr.*, vol. 23, no. 2, pp. 265–271, Mar. 1999.

[18] V. D. Calhoun *et al.*, "Semi-blind ICA of fMRI: A method for utilizing hypothesis-derived time courses in a spatial ICA analysis," *Neuroimage*, vol. 25, no. 2, pp. 527–538, Apr. 2005.

[19] Q. H. Lin *et al.*, "Semiblind spatial ICA of fMRI using spatial constraints," *Human Brain Map.*, vol. 31, no. 7, pp. 1076–1088, Dec. 2009.

[20] K. Lee, S. Tak, and J. C. Ye, "A data-driven sparse GLM for fMRI analysis using sparse dictionary learning with MDL criterion," *IEEE Trans. Med. Imag.*, vol. 30, no. 5, pp. 1076–1089, May 2011.

[21] M. D. Greicius, B. Krasnow, A. L. Reiss, and V. Menon, "Functional connectivity in the resting brain: A network analysis of the default mode hypothesis," *PNAS*, vol. 100, no. 1, pp. 253–258, Jan. 2003.

[22] P. Fransson, "Spontaneous low-frequency BOLD signal fluctuations: An fMRI investigation of the resting-state default mode of brain function hypothesis," *Human Brain Map.*, vol. 26, no. 1, pp. 15–29, Apr. 2003.

[23] I. Daubechies *et al.*, "Independent component analysis for brain fMRI does not select for independence," *PNAS*, vol. 106, no. 26, pp. 10415–10422, Apr. 2009.

[24] M. J. McKeown and T. J. Sejnowski, "Independent component analysis of fMRI data: Examining the assumptions," *Human Brain Map.*, vol. 6, pp. 368–372, 1998.

[25] J. Mairal, F. Bach, J. Ponce, G. Sapiro, and G. , "Online learning for matrix factorization and sparse coding," *J. Mach. Learn. Res.*, vol. 11, pp. 19–60, Mar. 2010.

[26] J. Wright, A. Y. Yang, A. Ganesh, S. Sastry, and Y. Ma, "Robust face recognition via sparse representation," *IEEE Trans. Pattern Anal. Mach. Intell.*, vol. 31, no. 2, pp. 210–227, Feb. 2009.

[27] J. Yang, J. Wright, T. S. Huang, and Y. Ma, "Image super-resolution via sparse representation," *IEEE Trans. Image Process.*, vol. 19, no. 11, pp. 2861–2873, Nov. 2010.

[28] J. Wright *et al.*, "Sparse representation for computer vision and pattern recognition," *Proc. IEEE*, vol. 98, no. 6, pp. 1031–1044, Jun. 2010.

[29] B. A. Olshausen, "Emergence of simple-cell receptive field properties by learning a sparse code for natural images," *Nature*, vol. 381, no. 6583, pp. 607–609, Jun. 1996.

[30] R. Q. Quiroga *et al.*, "Sparse but not 'grandmother-cell' coding in the medial temporal lobe," *Trends Cognitive Sci.*, vol. 12, no. 3, pp. 87–91, Mar. 2008.

[31] R. Q. Quiroga *et al.*, "Invariant visual representation by single neurons in the human brain," *Nature*, vol. 435, no. 7045, pp. 1102–1107, Feb. 2005.

[32] M. Aharon, M. Elad, M. , and A. Bruckstein, "k-svd: An algorithm for designing overcomplete dictionaries for sparse representation," *IEEE Trans. Signal Process.*, vol. 54, no. 11, pp. 4311–4322, Nov. 2006.

[33] M. Lewicki, M. , T. Sejnowski, and T. , "Learning overcomplete representations," *Neural Comput.*, vol. 12, no. 2, pp. 337–365, Feb. 2000.

[34] K. Kreutz-Delgado *et al.*, "Dictionary learning algorithms for sparse representation," *Neural Comput.*, vol. 15, no. 2, pp. 349–396, Feb. 2003.

[35] B. Gaonkar, K. Pohl, and C. Davatzikos, "Pattern based morphometry," Medical Image Computing and Computer-Assisted Intervention-MICCAI 2011 pp. 459–466, Sep. 2011 [Online]. Available: http://link.springer.com/chapter/10.1007/978-3-642-23629-7_56

[36] L. Su *et al.*, "Sparse representation of brain aging: Extracting covariance patterns from structural MRI," *PloS One*, vol. 7, no. 5, pp. 1–13, May 2012.

[37] Y. Li, A. Cichocki, and S. I. Amari, "Analysis of sparse representation and blind source separation," *Neural Comput.*, vol. 16, no. 6, pp. 1193–1234, Jun. 2004.

[38] Q. Barthélemy *et al.*, "Multivariate temporal dictionary learning for EEG," *J. Neurosci. Methods*, vol. 215, no. 1, pp. 19–28, Apr. 2013.

[39] Y. Shin, S. Lee, J. Lee, and H. N. Lee, "Sparse representation-based classification scheme for motor imagery-based brain—Computer interface systems," *J. Neural Eng.*, vol. 9, no. 5, pp. 1–12, Oct. 2012.

[40] B. Hamner, R. Chavarriaga, and J. D. R. Millán, "Learning dictionaries of spatial and temporal EEG primitives for brain-computer interfaces," in *Workshop on Structured Sparsity: Learning and Inference, ICML*, 2011, EPFL-CONF-166740.

[41] Y. Li *et al.*, "Voxel selection in fMRI data analysis based on sparse representation," *IEEE Trans. Biomed. Eng.*, vol. 56, no. 10, pp. 2439–2451, Oct. 2009.

[42] Y. Li *et al.*, "A sparse representation-based algorithm for pattern localization in brain imaging data analysis," *PloS One*, vol. 7, no. 12, Dec. 2012.

[43] J. Lee, Y. Jeong, and J. C. Ye, "Group sparse dictionary learning and inference for resting-state fMRI analysis of Alzheimer's disease," in *Proc. IEEE 10th Int. Symp. Biomed. Imag.*, Apr. 2013, pp. 540–543.

[44] V. P. Oikonomou, K. Blekas, and L. Astrakas, "A sparse and spatially constrained generative regression model for fMRI data analysis," *IEEE Trans. Biomed. Eng.*, vol. 59, no. 1, pp. 58–67, Jan. 2012.

[45] O. Yamashita, M. A. Sato, T. Yoshioka, F. Tong, and Y. Kamitani, "Sparse estimation automatically selects voxels relevant for the decoding of fMRI activity patterns," *Neuroimage*, vol. 42, no. 4, pp. 1414–1429, Oct. 2008.

[46] A. Julazadeh, J. Alirezaie, and P. Babyn, "A novel automated approach for segmenting lateral ventricle in MR images of the brain using sparse representation classification and dictionary learning," in *Proc. 11th Int. Conf. Inf. Sci., Signal Process. Appl.*, Jul. 2012, pp. 888–893.

[47] Y. H. Kim, J. Kim, and J. Lee, "Iterative approach of dual regression with a sparse prior enhances the performance of independent component analysis for group functional magnetic resonance imaging (fMRI) data," *Neuroimage*, vol. 63, no. 4, pp. 1864–1889, Aug. 2012.

[48] X. Zhang *et al.*, "Characterization of task-free and task-performance brain states via functional connectome patterns," *Med. Image Anal.*, vol. 17, no. 8, pp. 1106–1122, Dec. 2013.

[49] V. Abolghasemi, S. Ferdowsi, and S. Sanei, "Fast and incoherent dictionary learning algorithms with application to fMRI," *Signal, Image Video Process.*, pp. 1–12, Feb. 2013.
[50] H. Eavani, R. Filipovych, and C. Davatzikos, "Sparse dictionary learning of resting state fMRI networks," in *Proc. Int. Workshop Pattern Recognit. NeuroImag.*, 2012, pp. 73–76.
[51] N. Wang, W. Zeng, L. Chen, and L. , "SACICA: A sparse approximation coefficient-based ICA model for functional magnetic resonance imaging data analysis," *J. Neurosci. Methods*, vol. 216, no. 1, pp. 49–61, May 2013.
[52] M. Ramezani *et al.*, "Joint sparse representation of brain activity patterns in multi-task fMRI data," *IEEE Trans. Med. Imag.*, vol. 34, pp. 2–12, 1, Jul. 2014.
[53] S. Zhang, X. Li, and T. Liu, "Sparse representation of higher-order functional interaction patterns in task-based FMRI data," Medical Image Computing and Computer-Assisted Intervention-MICCAI 2013 Sep. 2013 [Online]. Available: http://link.springer.com/chapter/10.1007/978-3-642-40760-4_78
[54] J. L. Lv *et al.*, "Holistic atlases of functional networks and interactions reveal reciprocal organizational architecture of cortical function," *IEEE Trans. Biomed. Eng.*, vol. 62, no. 4, pp. 1120–1131, Apr. 2015.
[55] J. L. Lv *et al.*, "Sparse representation of whole-brain fMRI signals for identification of functional networks," *Med. Image Anal.*, Feb. 2015.
[56] J. Duncan, "The multiple-demand (MD) system of the primate brain: Mental programs for intelligent behavior," *Trends Cognitive Sci.*, vol. 14, no. 4, pp. 172–179, Apr. 2010.
[57] M. S. Gazzaniga, *The Cognitive Neurosciences*, 3rd ed. Cambridge, MA: MIT.
[58] L. Pessoa, "Beyond brain regions: Network perspective of cognition—Emotion interactions," *Behav. Brain Sci.*, vol. 35, no. 3, pp. 158–159, May 2012.
[59] G. Varoquaux, A. Gramfort, and B. Thirion, "Multi-subject dictionary learning to segment an atlas of brain spontaneous activity," Information Processing in Medical Imaging [Online]. Available: link.springer.com/chapter/10.1007/978-3-642-22092-0_46#page-1 Jan. 2011
[60] D. M. Barch *et al.*, "Function in the human connectome: Task-fMRI and individual differences in behavior," *Neuroimage*, vol. 80, pp. 169–189, Oct. 2013.
[61] A. R. Hariri *et al.*, "The amygdala response to emotional stimuli: A comparison of faces and scenes," *Neuroimage*, vol. 17, no. 1, pp. 317–323, Sept. 2002.
[62] M. R. Delgado *et al.*, "Tracking the hemodynamic responses to reward and punishment in the striatum," *J. Neurophysiol.*, vol. 84, no. 6, pp. 3072–3077, Dec. 2000.
[63] J. R. Binder *et al.*, "Mapping anterior temporal lobe language areas with fMRI: A multicenter normative study," *Neuroimage*, vol. 54, no. 2, pp. 1465–1475, Jan. 2011.
[64] R. L. Buckner *et al.*, "The organization of the human cerebellum estimated by intrinsic functional connectivity," *J. Neurophysiol.*, vol. 106, no. 5, pp. 2322–2345, Nov. 2011.
[65] B. T. Yeo *et al.*, "The organization of the human cerebral cortex estimated by intrinsic functional connectivity," *J. Neurophysiol.*, vol. 106, no. 3, pp. 1125–1165, Nov. 2011.
[66] R. Smith, K. Keramatian, and K. Christoff, "Localizing the rostrolateral prefrontal cortex at the individual level," *Neuroimage*, vol. 36, no. 4, pp. 1387–1396, Jul. 2007.
[67] F. Castelli, C. Frith, F. Happé, U. Frith, and U. , "Autism, asperger syndrome and brain mechanisms for the attribution of mental states to animated shapes," *Brain*, vol. 125, no. 8, pp. 1839–1849, 2002.
[68] T. Wheatley, S. C. Milleville, and A. Martin, "Understanding animate agents distinct roles for the social network and mirror system," *Psychol. Sci.*, vol. 18, no. 6, pp. 469–474, Jun. 2007.
[69] S. J. White, D. Coniston, and U. Frith, "Developing the Frith-Happé animations: A quick and objective test of theory of mind for adults with autism," *Autism Res.*, vol. 4, no. 2, pp. 149–154, Jan. 2011.
[70] X. Lu, H. Yuan, and X. Li, "Geometry constrained sparse coding for single image super-resolution," in *Proc. IEEE Conf. Comput. Vis. Pattern Recognit.*, Jun. 2012.
[71] M. Zheng *et al.*, "Graph regularized sparse coding for image representation," *IEEE Trans. Image Process.*, vol. 20, no. 5, pp. 1327–1336, May 2011.
[72] J. Lee, M. Fukunaga, and J. H. Duyn, Sparse decoding in fMRI 2008 [Online]. Available: http://cds.ismrm.org/ismrm-2008/files/02481.pdf
[73] J. Gonzalez-Castillo *et al.*, "Whole-brain, time-locked activation with simple tasks revealed using massive averaging and model-free analysis," *PNAS*, vol. 109, no. 14, pp. 5487–5492, 2012.
[74] S. M. Smith, P. T. Fox, and C. F. Beckmann, "Correspondence of the brain's functional architecture during activation and rest," *PNAS*, vol. 106, no. 31, pp. 13040–13045, 2009.
[75] C. F. Beckmann, M. DeLuca, J. T. Devlin, and S. M. Smith, "Investigations into resting-state connectivity using independent component analysis," *Phil. Trans. R. Soc. London B, Biol. Sci.*, vol. 360, no. 1457, pp. 1001–1013, May 2005.
[76] J. Huang, S. Zhang, H. Li, and D. Metaxas, "Composite splitting algorithms for convex optimization," *Comput. Vis. Image Understand.*, vol. 115, no. 12, pp. 1610–1622, 2011.
[77] J. Huang, S. Zhang, and D. Metaxas, "Efficient MR image reconstruction for compressed MR imaging," *Med. Image Anal.*, vol. 15, no. 5, pp. 670–679, 2011.
[78] J. Caballero, A. N. Price, D. Rueckert, and J. V. Hajnal, "Dictionary learning and time sparsity for dynamic MR data reconstruction," *IEEE Trans. Med. Imag.*, vol. 33, no. 4, pp. 979–994, Mar. 2014.